Journal of Power Sources 354 (2017) 172–178

Contents lists available at ScienceDirect

Journal of Power Sources

journal homepage: www.elsevier.com/locate/jpowsour

Enhanced rate performance of $Li_4Ti_5O_{12}$ anodes with bridged grain boundaries

Xu-Yong Feng [a, c], Xiang Li [a], Mingxue Tang [a, b], Alberic Gan [d], Yan-Yan Hu [a, b, *]

[a] Department of Chemistry and Biochemistry, Florida State University, Tallahassee, FL, 32306, USA
[b] Centre of Interdisciplinary Magnetic Resonance, National High Magnetic Field Laboratory, 1800 East Paul Dirac Drive, Tallahassee, FL, 32310, USA
[c] School of Materials Science and Engineering, Hefei University of Technology, Anhui, 230009, PR China
[d] Lawton Chiles High School, 7200 Lawton Chiles Ln, Tallahassee, FL, 32312, USA

HIGHLIGHTS

- Bridged grain boundaries are beneficial for good rate performance of LTO.
- High-temperature treatment of short duration promotes grain boundary formation.
- NMR follows Li evolution induced by electrochemical cycling.

ARTICLE INFO

Article history:
Received 9 November 2016
Received in revised form
12 March 2017
Accepted 8 April 2017

Keywords:
Lithium-ion battery
Lithium titanium oxide
Solid-state NMR
Grain boundary

ABSTRACT

Excellent rate performance of $Li_{4+x}Ti_5O_{12}$ ($0 < x < 3$, LTO) electrodes results from mixed Li site occupancy and facile Li ion exchange at 8a and 16c sites. In this paper, we reveal that inter-particle connectivity within LTO electrodes affects 8a and 16c site occupancies upon discharge and impacts Li ion diffusion. LTO electrodes of the same primary crystal structure but of different grain boundary structures were prepared and they showed significantly different electrochemical performance. LTO electrodes with a percolated 3D structural network and bridged grain boundaries offered balanced 8a-16c occupancy, Li ion exchange at 8a and 16c sites upon discharge, high ionic conductivities, and good rate performance. While LTO electrodes with isolated clusters of particles showed strong rate dependence of 8a-16c occupancy, a lack of Li ion exchange at 8a and 16c sites, large over-potential, and substantial capacity decay upon fast charging. Bridged grain boundaries in LTO secondary particles facilitate apparent solid-solution process during electrochemical cycling by maintaining Li site exchange and thus enhance the rate performance of LTO electrodes.

1. Introduction

High rate performance of rechargeable Li ion batteries (LIBs) is highly desirable in high-power energy storage applications [1–5]. The formation of phase boundaries in battery electrode materials is often associated with poor rate performance. However, two exceptions are $Li_4Ti_5O_{12}$ and $LiFePO_4$, which despite showing a first-order phase transition, offer excellent rate performance and stable long-term cycling [5–11]. Debates regarding these two exceptional systems center around the fundamental nature of the structural change, whether it is a solid solution, a phase separation on different length scales, or a combination of the two depending on the particle size of electrodes and battery cycling conditions [7,12–17]. For the two-phase reaction mechanism, it has been proposed that the grain boundary, in the case of $Li_4Ti_5O_{12}$, facilitates ion and electron transport instead of impeding it, which explains the low activation energy for fast ion transport in the intermediate region of discharge with a composition $Li_{4+x}Ti_5O_{12}$ ($0 < x < 3$) [18]. The effects of grain boundaries on charge carrier transport and the rate performance of $Li_4Ti_5O_{12}$ have been extensively investigated. Both computational and experimental efforts have been invested to resolve the puzzle of phase separation vs. solid solution [7,18].

Experimental studies [19–21] on Li ion dynamics and diffusion pathways in $Li_{4+x}Ti_5O_{12}$ ($0 \leq x \leq 3$) have provided the following

* Corresponding author. Department of Chemistry and Biochemistry, Florida State University, Tallahassee, FL, 32306, USA.
E-mail address: hu@chem.fsu.edu (Y.-Y. Hu).

http://dx.doi.org/10.1016/j.jpowsour.2017.04.032
0378-7753/

insights: i) spinel $Li_4Ti_5O_{12}$ is a poor Li ion conductor with a site occupancy $[Li]_{8a}[Ti_{5/3}Li_{1/3}]_{16d}[O_4]_{32e}$, ii) Li ion diffusivity increases at early stage lithiation ($x < 0.3$) and decrease with further lithiation beyond $x = 0.3$, followed by continuous decrease in Li ion diffusivity with $x > 0.3$, and iii) fully lithiated $Li_7Ti_5O_{12}$ has a rock salt structure with a site occupancy of $[Li_2]_{16c}[Ti_{5/3}Li_{1/3}]_{16d}[O_4]_{32e}$. $Li_7Ti_5O_{12}$ is a mixed ion-electron conductor, with higher Li ion diffusivity than $Li_4Ti_5O_{12}$ but lower than $Li_{4+x}Ti_5O_{12}$ ($0 < x < 3$). Diffraction measurements reveal that $Li_{4+x}Ti_5O_{12}$ stays as a single phase at equilibrium, and fast lithiation or de-lithiation promotes the two-phase reaction but relax to a solid-solution state with time [7]. Mixed 8a and 16c Li occupancy is credited for the formation of apparent solid solution, and thus for the excellent rate performance of $Li_{4+x}Ti_5O_{12}$ ($0 < x < 3$).

In this paper, we report observations regarding the effects of bridged grain boundaries on maintaining the occupancy balance between 8a and 16c sites in LTO structures, and the associated impact on rate performance and over-potentials of LIBs using LTO electrodes. Pristine $Li_4Ti_5O_{12}$ has been prepared with two different Li-containing precursors (Li_2CO_3 and CH_3COOLi, LiAc) or different heat treatment, which exhibit the same crystal structure as characterized by X-ray diffraction and high-resolution solid-state Li NMR, but show different morphologies, as revealed by scanning electron microscopy (SEM). The 3D bridged network of LTO particles results in a relatively constant 8a and 16c occupancy with variable rate discharging and minimal over-potential upon fast charging. In contrast, isolated small clusters of LTO particles lead to changes in the 8a/16c occupancy ratio when discharged at different rates, due to the lack of 8a-16c Li exchange observed by NMR. As a result, the low ionic conductivity of LTO electrodes with isolated particles yields significant over-potential for fast-rate electrochemical cycling. In summary, this paper investigates the impact of grain boundaries in LTO electrodes on altering the crystal structure, site occupancy, and Li ion transport properties upon battery cycling.

2. Experimental

2.1. Material preparation

Two different LTO samples were synthesized using TiO_2 and different lithium sources (Li_2CO_3 and LiAc) with the same calcining temperature. A mixture of TiO_2 and Li_2CO_3 (or LiAc), with a molar ratio of Li: Ti = 4.2 : 5.0 was hand ground for 30 min. The mixture was then calcined at 500 °C for 5 h and 800 °C for 10 h to ensure complete reaction. For convenience, LTO/Li_2CO_3 and LTO/LiAc were used to denote the samples synthesized with Li_2CO_3 and CH_3COOLi, respectively.

2.2. Electrochemistry

$Li_4Ti_5O_{12}$, acetylene black, and polyvinylidene fluoride (pvdf) dissolved in *N*-methyl-2-pyrrolidinone were mixed together to form a homogenous slurry, which was then cast on a piece of carbon coated copper foil. After drying at 100 °C, the electrode film was punched into discs with a diameter of 12.5 mm. The prepared electrode contains 80 wt% $Li_4Ti_5O_{12}$, 10 wt% acetylene black, and 10 wt% pvdf. Loading of $Li_4Ti_5O_{12}$ on each disc was 2–3 mg. The electrochemical performance of LTO electrodes was measured using CR2032 coin cells with Li metal as the counter electrode. The cells were assembled in an argon-filled dry-box (MBraun) with a microporous membrane (Celgard, K2045) as the separator, and 1 M $LiPF_6$ in EC/DMC/DEC (w/w = 1:1:1) as the electrolyte. They were cycled on a multi-channel battery test system (LAND) within a voltage range of 1.0 V–2.5 V. Cyclic voltammetry (CV) on these batteries was measured at room temperature on a Reference 600 (Gamry Instruments).

2.3. X-ray diffraction, scanning electron microscopy, and electrode surface area measurement

The crystal structures of these $Li_4Ti_5O_{12}$ samples were determined by X-ray diffraction (XRD) (X'PERT Pro MPD, Cu Kα radiation, λ = 0.15406 nm). The diffraction patterns were recorded at room temperature in the 2θ range from 10° to 80°, with a scan rate of 7°/min. The morphology and particle size of $Li_4Ti_5O_{12}$ samples were characterized with scanning electron microscopy (SEM, Nova 400 Nano, FEI). Electrode surface area measurements were performed on a Micromeritics TriStar 3000 surface area and porosity analyzer using nitrogen adsorption method.

2.4. NMR spectroscopy

Pristine LTO samples were packed into 1.3-mm rotors inside an Argon glovebox before acquiring NMR spectra. The ^7Li magic angle spinning (MAS) NMR spectra were acquired on an Avance III Bruker spectrometer using a 1.3-mm MAS probe in a 14.7 T magnetic field, with a ^7Li Larmor frequency of 233.1 MHz. ^7Li spectra were obtained using a rotor-synchronized spin-echo sequence at a MAS rate of 50 kHz. The 90° pulse length was 1 μs and the recycle delay was 15 s. ^7Li shifts were referenced to LiF at −1 ppm.

The cycled LTO electrodes were washed with dimethyl carbonate (DMC) 3 times to ensure the removal of residual electrolytes. DMC was removed by vacuum drying before NMR characterizations. As the discharge voltage was limited to 1 V, no significant solid-electrolyte-interphase (SEI) formation is expected on the surface of LTO electrodes.

^7Li MAS NMR experiments on cycled LTO electrodes were performed on a Bruker AVANCE III spectrometer with a 2.5-mm MAS probe in a magnetic field of 11.75 T. The Larmor frequency of ^7Li was 194.3 MHz. A rotor-synchronized spin-echo pulse was employed at a MAS rate of 25 kHz. The 90° pulse length was 5 μs and the recycle delay was 2 s. Solid LiCl with a ^7Li shift at 1.1 ppm was used as a reference. The ^7Li NMR spectra simulations were carried out using the dmfit software [22].

3. Results and discussions

SEM images of LTO/Li_2CO_3 and LTO/LiAc in Fig. 1a and b show that primary LTO/LiAc particles aggregate to loosely packed small clusters while LTO/Li_2CO_3 particles of submicron size are connected to form a percolated network. When using Li_2CO_3 as the lithium source, it starts to melt at 723 °C, which helps the growth of grain boundaries (red circle in Fig. 1a) among $Li_4Ti_5O_{12}$ particles. LiAc decomposes to lithium oxides with a very high melting point before converting to $Li_4Ti_5O_{12}$. At 800 °C, the lack of intermediate liquid phase yields loose particles aggregates. Further examination on the crystal structures of LTO/LiAc and LTO/Li_2CO_3 was carried out using solid-state ^7Li NMR and X-ray diffraction. ^7Li NMR of both LTO/LiAc and LTO/Li_2CO_3 revealed a major resonance at 0.08 ppm with a shoulder on the left at −0.26 ppm. Based on the spectral simulation and previous NMR studies of LTO [19,20], the 0.08-ppm resonance was assigned to Li at 8a sites and the −0.26 ppm resonance was assigned to Li at 16d sites. The ratio of $[Li]_{8a}$: $[Li]_{16d}$ is 3:1 in both LTO/LiAc and LTO/Li_2CO_3, consistent with the stoichiometry of $Li_4Ti_5O_{12}$, *i.e.*, $[Li]_{8a}[Ti_{5/3}Li_{1/3}]_{16d}[O_4]_{32e}$. The XRD patterns of LTO/LiAc and LTO/Li_2CO_3 were identical (Fig. S1). Therefore, SEM, NMR, and XRD results revealed the same crystal structure but different morphologies of LTO/LiAc and LTO/Li_2CO_3 pristine electrodes.

Ex situ ^7Li NMR was performed to follow structure and phase transitions of LTO used in half-cell batteries at different states of

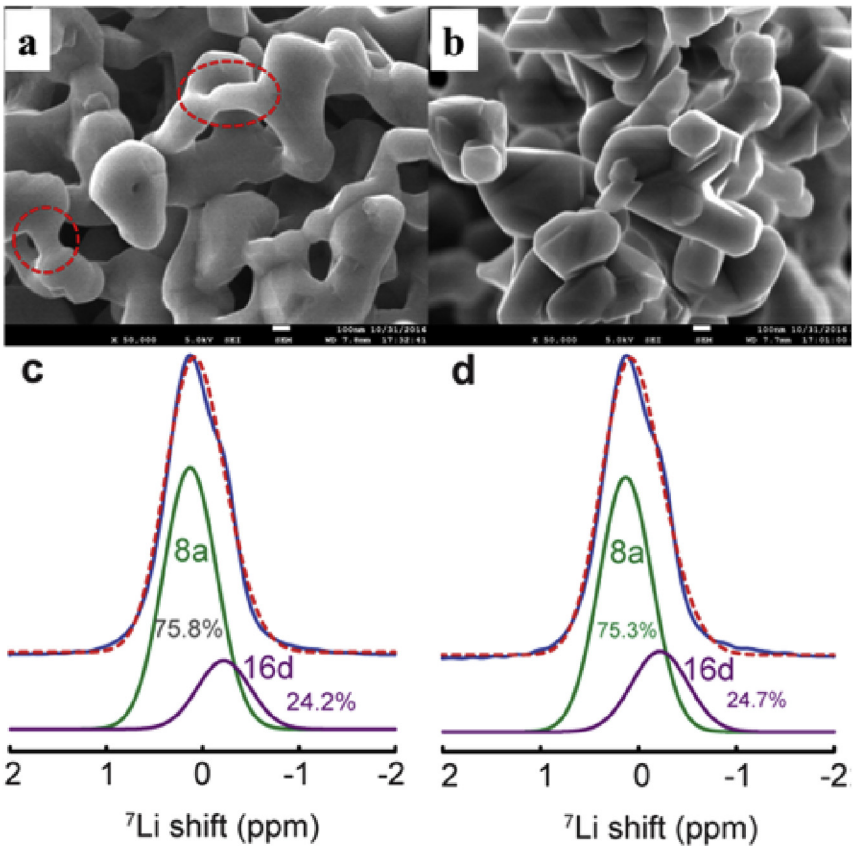

Fig. 1. SEM images of LTO/Li_2CO_3 (a) and LTO/LiAc (b) with a scale bar of 100 nm. ^{7}Li NMR of LTO/Li_2CO_3 (c) and LTO/LiAc (d). Blue plots represent experimental spectra, while the purple/green plots represent simulated spectra. The sums of the simulated spectra are shown in red. The fraction of each subcomponent in the total spectra is indicated. (For interpretation of the references to colour in this figure legend, the reader is referred to the web version of this article.)

charge. The electrochemical profile of an LTO/Li half-cell battery cycled at a rate of C/16 (11 mA/g) is shown in Fig. 2a. A plateau occurs around 1.55 V for both charge and discharge with very small hysteresis. ^{7}Li NMR spectra at different states of (dis)charge denoted as P, D1, D2, C1, and C2 in Fig. 2a are displayed in Fig. 2b. The ^{7}Li NMR spectrum of pristine LTO (P at the bottom of Fig. 2b) shows two partially overlapped peaks around 0 ppm from Li at 8a and 16d sites. Upon discharge, a broad low-lying resonance centered at −10 ppm emerges, assigned to Li at 16c sites. The broad 16c resonance grows stronger as the discharge process proceeds until the end at 1.0 V. This indicates the gradual insertion of Li ions into 16c sites of LTO. In addition, the intensity of the 8a resonance decreases, suggesting Li migration from 8a to 16c. These two processes, direct Li insertion into 16c sites and Li migration from 8a to 16c, lead to the eventual phase transformation of spinel $Li_4Ti_5O_{12}$ to rock salt $Li_7Ti_5O_{12}$ at the end of discharge. The charging process is the reverse of the discharge process, manifested in Fig. 2b as the decrease and disappearance of the 16c resonance at −10 ppm and the return of the 8a NMR peak around 0 ppm.

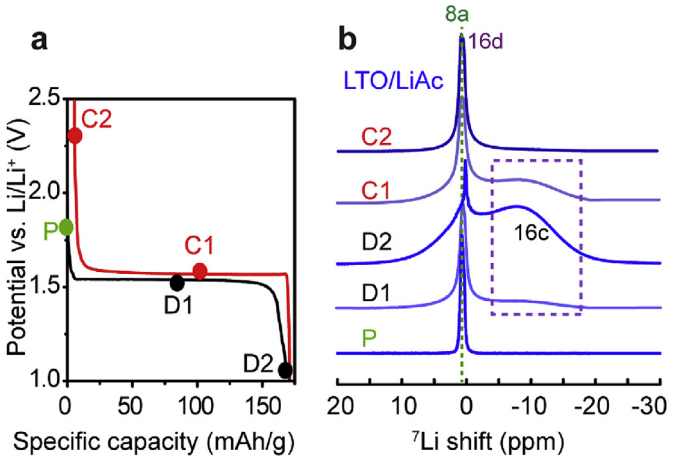

Fig. 2. a) Electrochemical profile of a typical LTO/Li half-cell battery, b) *ex situ* high-resolution ^{7}Li NMR of cycled LTO electrodes at different states of charge as indicated in a). P represents pristine LTO electrode.

The first-order $Li_4Ti_5O_{12}$-$Li_7Ti_5O_{12}$ phase transition occurs at 1.55 V with a very small over-potential at a slow cycling rate. Over-potentials for both discharge and charge increase with increasing cycling rates. LTO/Li_2CO_3 and LTO/LiAc electrodes display different behaviors (Fig. 3), regarding over-potentials at fast charging. These half-cells were discharged at a rate of 1C and charged at 1C, 4C, 8C, and 16C. Fig. 3a shows very small over-potential even at 16C, and minimal capacity decay is observed for batteries using LTO/Li_2CO_3 electrodes. In contrast, Fig. 3b shows a gradual increase in over-potential when the charging rate was increased from 1C to 16C, and noticeable capacity decay occurs at 16C. For clearer comparison, the plots of average charge voltage *vs.* C rate for batteries using LTO/Li_2CO_3 and LTO/LiAc electrodes are shown in Fig. 3c. A linear increase of the average charge potential (*vs.* Li/Li^+) with increasing C rate is seen for both LTO/Li_2CO_3 and LTO/LiAc electrodes, and the slope is greater for LTO/LiAc than for LTO/Li_2CO_3. In addition to over-potential, rate performance of electrodes can also be gauged based on capacity variation upon cycling with different rates. As

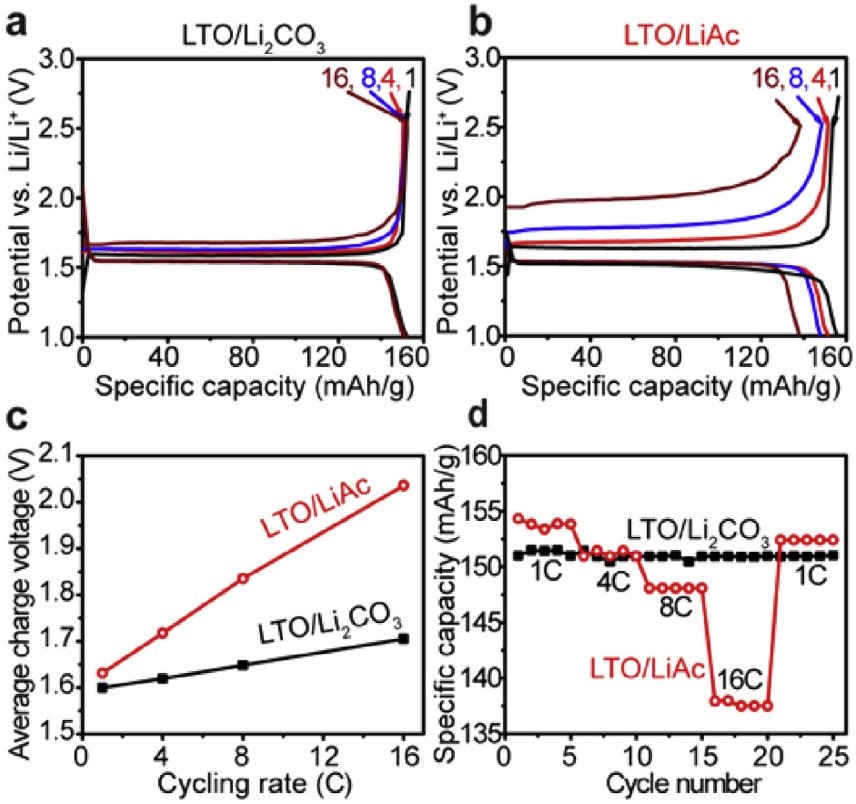

Fig. 3. Electrochemical profiles of LTO/Li batteries discharged at 1C and charged at different rates of 1C, 4C, 8C, and 16C with LTO electrodes made from precursors of a) Li_2CO_3, b) LiAc, the average charge voltage (c) and rate performance (d) of LTO/Li batteries.

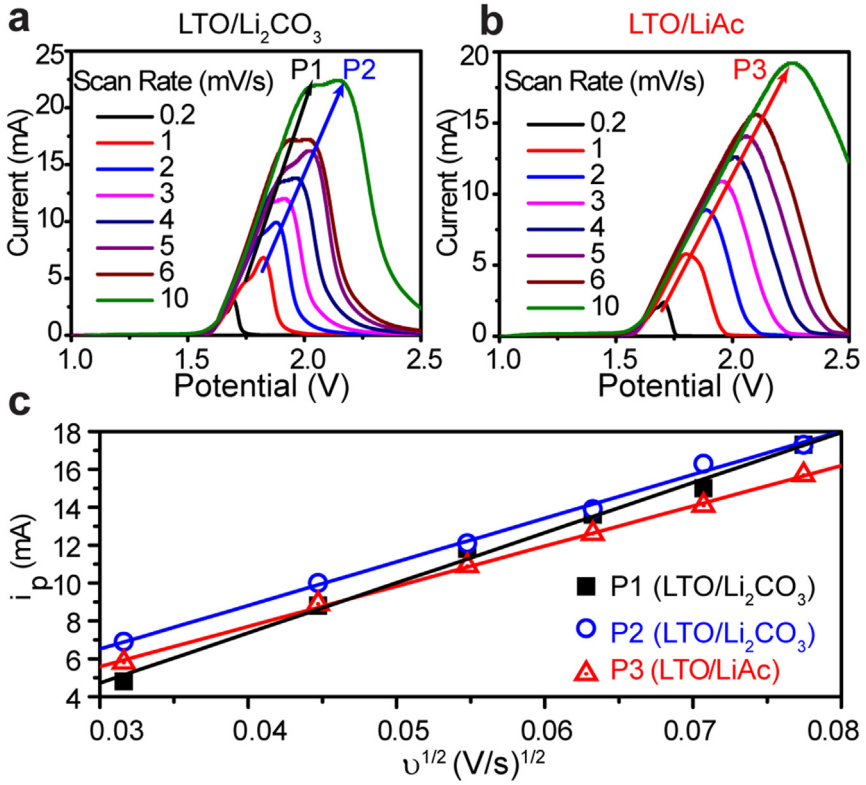

Fig. 4. Cyclic voltammetry of half-cell batteries employing a) LTO/Li_2CO_3 and b) LTO/LiAc electrodes. Only the charge process with varying voltage-scanning rate is shown, the discharge scanning rate was fixed at 0.2 mV/s c) a plot of the peak current i_p *vs.* the square root of voltage scanning rate. Two distinct processes P1 and P2 were identified for the LTO/Li_2CO_3 electrodes, and one process P3 for the LTO/LiAc electrodes.

seen in Fig. 3d, the specific capacity for LTO/Li_2CO_3 electrodes stayed almost constant with increasing charge rate, however, substantial reduction in specific capacity is correlated with fast charging for LTO/LiAc electrodes. Overall, LTO/Li_2CO_3 electrodes exhibit significantly better rate performance compared with LTO/LiAc electrodes.

The difference between LTO/Li_2CO_3 and LTO/LiAc electrodes in terms of electrochemical performance can be further probed with cyclic voltammetry (CV). Fig. 4a and b show the CV profiles with increased scanning rate from 0.2 mV/s to 10 mV/s in the positive direction for half-cells employing LTO/Li_2CO_3 and LTO/LiAc electrodes. The scanning rate in the negative direction is kept constant at 0.2 mV/s. Two distinct processes are seen for the LTO/Li_2CO_3 electrode, while only one is resolved for LTO/LiAc. To more clearly illustrate this difference, the peak current i_p (mA) is plotted against the square root of voltage scanning rate (V/s) and the plot is presented in Fig. 4c. For Faradaic processes, i_p and $\nu^{1/2}$ are linearly correlated [23],

$$i_p = \left(2.69 \times 10^5\right) n^{3/2} A D_{Li^+}^{1/2} C_{Li} \nu^{1/2} \quad (1)$$

n: number of electrons on each charge carrier, n = 1 for Li^+.
A (cm^2): surface area of the electrode.
C_{Li} (moles/cm^3): bulk concentration of Li^+ in electrodes (0.03).
D_{Li^+} (cm^2/s): Li^+ diffusivity.

The specific surface area was determined, based on N_2 absorption, to be 2.46 m^2/g for LTO/Li_2CO_3 and 4.80 m^2/g for LTO/LiAc. The relatively larger specific surface area for LTO/LiAc is consistent with the observation with SEM that the particle size for LTO/Li_2CO_3 and LTO/LiAc electrodes is similar but LTO/Li_2CO_3 exhibits more grain boundaries thus reduced specific surface area. The mass for both LTO/Li_2CO_3 and LTO/LiAc electrodes is 2.12 mg. Therefore, according to equation (1), one of the two processes (P1) shown for LTO/Li_2CO_3 electrodes has a slightly higher Li^+ diffusivity of 3.32×10^{-13} cm^2 s^{-1} than the other process (P2), 2.52×10^{-13} cm^2 s^{-1}. Li^+ diffusivity in LTO/LiAc (P3) is calculated to be 5.62×10^{-14} cm^2 s^{-1}. It is worth mentioning that closer examination of the CV profile for LTO/LiAc electrodes also reveals two processes. However, due to relatively sluggish ion and electron transport at high scanning rates, only one linear i_p-$\nu^{1/2}$ correlation curve is resolved. In addition, the Li^+ diffusivity was also measured with the Ac impedance at different charge depth and the LTO/Li_2CO_3 also shows ~5 times higher average Li^+ diffusivity (Table S1) compared with LTO/LiAc.

Factors accounting for the difference in Li ion conduction LTO/Li_2CO_3 and LTO/LiAc electrodes upon charge can be traced back to the characteristics of $Li_{4+x}Ti_5O_{12}$ structures and Li occupancies. ^{7}Li NMR spectra of LTO/Li_2CO_3 and LTO/LiAc electrodes discharged to 1V with different rates were used to show Li occupancy variation

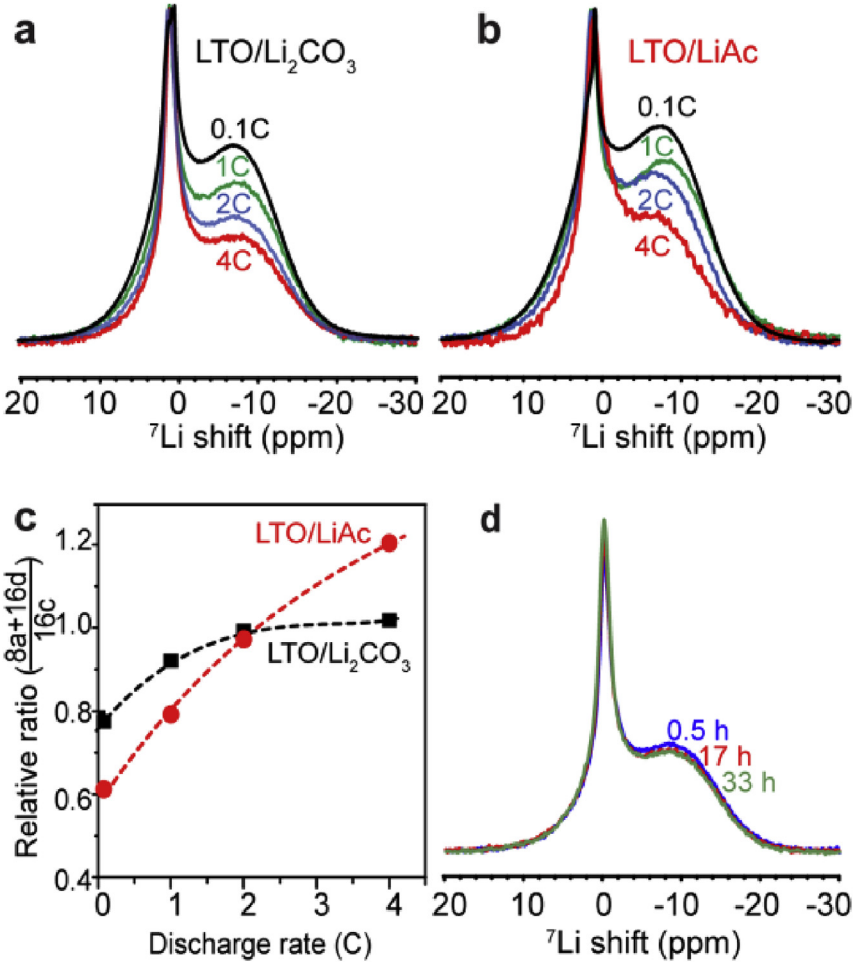

Fig. 5. ^{7}Li NMR of a) LTO/Li_2CO_3 and b) LTO/LiAc electrodes discharged to 1 V at 0.1C, 1C, 2C, and 4C rates, c) the ratio of Li at 8a and 16d sites *vs.* 16c sites for electrodes discharged to 1 V against Li metal with different rates, and d) ^{7}Li spectra recorded at 0.5 h, 1 h, and 17 h after disassembling a fully discharged LTO/Li_2CO_3 electrode against Li metal at a rate of 4C.

(Fig. 5a and b). As the discharge rate was increased, 16c site occupancy decreases for both LTO/Li_2CO_3 and LTO/LiAc electrodes, but larger variation in the 8a site occupancy was observed for LTO/LiAc electrodes compared with LTO/Li_2CO_3 electrodes. For more quantitative analysis, the ratio of Li at 8a and 16d sites *vs.* Li at 16c site is calculated for both types of electrodes based on the area integral of ^{7}Li NMR spectra in Fig. 5a and b. The occupancy ratio plotted against discharge rate is presented in Fig. 5c. For LTO/Li_2CO_3 electrodes, the ratio of (8a+16d)/16c remains within a small range with different discharge rates of 0.1C, 1C, 2C, and 4C. At a low discharging rate of 0.1C, the (8a+16d)/16c ratio is 0.78, and with increasing discharge rates from 0.1C to 4C, the (8a+16d)/16c ratio only slightly increases and levels off around 1.00. In contrast, for LTO/LiAc electrodes, the (8a+16d)/16c ratio continuously increases from 0.6 at 0.1C to > 1.2 at 4C. The relatively un-regulated (8a+16d)/16c ratio in LTO/LiAc electrodes is likely from the lack of Li exchange between 8a and 16c sites. To test this hypothesis and to further explore Li ion exchange dynamics at 8a and 16c sites, LTO/Li_2CO_3 electrodes were prepared and cycled against Li metal at a rate of 4C until the end of discharge, the exchange between 8a and 16c was monitored with time-resolved ^{7}Li NMR. Selective ^{7}Li spectra at the time of 0.5, 17, and 33 h after disassembling the discharged battery are shown in Fig. 5d. The spectra reveal continuous decrease in the intensity of the 16c Li resonance and increase in the intensity of the 8a resonance with time, suggesting Li migration from 16c to 8a sites, consistent with previous neutron diffraction measurements [7]. On the other hand, similar migration from 16c to 8a was not observed in LTO/LiAc electrodes. Previous studies have concluded that Li exchange between 8a and 16c sites helps to reach apparent solid-solution state of LTO electrodes and prevent phase segregation on a macroscopic scale during fast charging [7]. Solid-solution state often exhibits much higher ionic and electronic conductivities compared with phase-segregated composites. Therefore, the observation of 8a-16c Li exchange likely contributes to the better rate performance of LTO/Li_2CO_3 electrodes compared to LTO/LiAc.

The crystal structures of pristine LTO/Li_2CO_3 and LTO/LiAc electrodes do not exhibit significant difference, as evidenced by similar ^{7}Li NMR spectra (Fig. 1c and d) and XRD patterns (Fig. S1). Simulation of the ^{7}Li NMR spectra reveals the stoichiometric composition, 25% Li at 16d sites and 75% at 8a sites, in both LTO/Li_2CO_3 and LTO/LiAc pristine electrodes. LTO/Li_2CO_3 and LTO/LiAc show very different morphologies, as observed with SEM. The SEM images in Fig. 1a and b shows that LTO/LiAc particles clustered in small groups while LTO/Li_2CO_3 particles form connected 3D structures with grain boundaries. The difference in grain boundaries affects the crystal structures of cycled LTO/Li_2CO_3 and LTO/LiAc electrodes significantly. In LTO/Li_2CO_3 electrodes, Li ion exchange between 8a and 16c sites helps to maintain a balance of Li

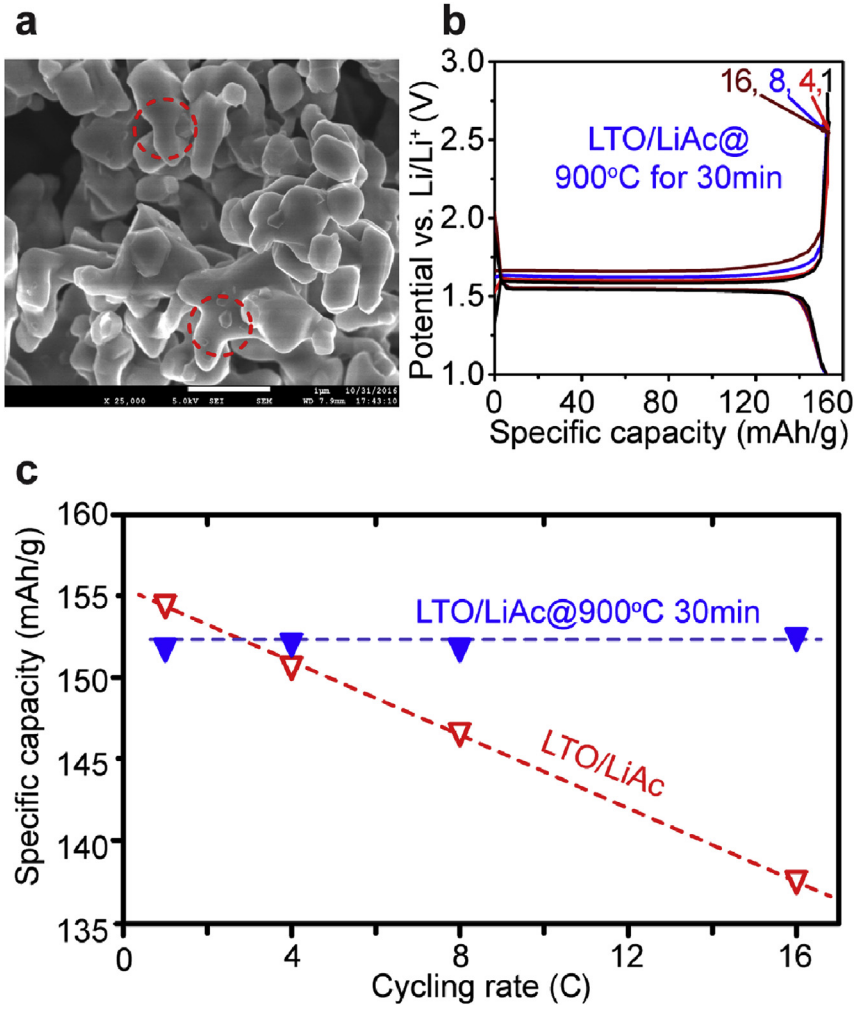

Fig. 6. a) SEM image of LTO/LiAc electrode sintered at 900 °C for 30 min., b) Electrochemical profile of LTO/LiAc electrodes sintered at 900 °C for 30 min. cycled against Li metal at a constant discharge rate of 1C and different charging rates of 1C, 4C, 8C, and 16C, and c) rate performance of LTO/LiAc electrodes without high-temperature sintering, and sintered at 900 °C for 30 min.

occupancies at these two sites, which prevents phase separation and also proves to be beneficial for fast ion conduction. In LTO/LiAc electrodes, the lack of Li exchange between 8a and 16c sites leads to imbalanced 8a and 16c site occupancies and results in early phase segregation. Higher Li diffusivity found in cycled LTO/Li_2CO_3 electrodes contributes to the observed lower over-potential at fast charging rates, compared with cycled LTO/LiAc electrodes.

Employing LiAc precursors for synthesizing LTO leads to the formation of small clusters of particles, likely due to the pyrolysis process of acetate groups. The secondary particles of LTO/LiAc electrodes can be modified by sintering at temperatures $\geq$900 °C. High-temperature sintering over a short period of time promotes the aggregation of smaller particle clusters and the establishment of a 3D structural network (Fig. 6a). As shown in Fig. 6b, sintering the LTO/LiAc electrode at 900 °C for 30 min significantly reduces the over-potential at fast charging and improves the rate performance of LTO/LiAc electrodes.

4. Conclusion

Two types of LTO electrodes with the same crystal structure but different grain boundary structures were studied to examine the effects of inter-particle connectivity on Li site occupancy and rate performance of cycled LTO electrodes used in rechargeable LIBs. The LTO electrodes with significant presence of grain boundaries demonstrated very small over-potential upon fast charging, while significant over-potential and capacity decay were observed for LTO electrodes made of isolated particles. The measured Li diffusivity in $Li_{4+x}Ti_5O_{12}$ is higher for LTO electrodes with connected particles compared with those with isolated LTO particles. High-resolution ^{7}Li NMR results have shown a larger extent of Li exchange between 8a and 16c sites in cycled LTO electrodes with connected particles compared with those of isolated particles. 8a-16c Li exchange in LTO electrodes prevents phase separation and supports good rate performance. It has been shown with this work that morphologies such as bridged grain boundaries and percolated structural networks induce changes on the crystal structure of cycled electrodes, which in turn affects the electrochemical performance of LTO anodes.

Conflict of interest

The authors declare no competing financial interest.

Acknowledgments

This work was supported by Florida State University through Hu Startup and the National Science Foundation under Grant No. DMR-1508404. Feng thanks National Science Foundation of China (51402289) for partial financial support with chemical purchase. All solid-state NMR experiments were carried out at the NHMFL supported by NSF under contract DMR-1157490. We also thank Heather Dang for proof reading and Prof. Jim Zheng and Dr. Qiang Wu from Florida State University for assistance with the electrode surface area measurements.

Appendix A. Supplementary data

Supplementary data related to this article can be found at http://dx.doi.org/10.1016/j.jpowsour.2017.04.032.

References

[1] T. Yuan, Y. Jiang, W. Sun, B. Xiang, Y. Li, M. Yan, B. Xu, S. Dou, Adv. Funct. Mater. 26 (2016) 2198–2206.
[2] M. Wang, G. Li, H. Xu, Y. Qian, J. Yang, ACS Appl. Mater. Interfaces 5 (2013) 1003–1008.
[3] Y. Zhang, L. Wang, Z. Guo, Y. Xu, Y. Wang, H. Peng, Angew. Chem. Int. Ed. 55 (2016) 4487–4491.
[4] S.M. Beladi-Mousavi, S. Sadaf, L. Walder, M. Gallei, C. Rüttiger, S. Eigler, C.E. Halbig, Adv. Energy Mater. 6 (2016) 1600108.
[5] X. Feng, H. Zou, H. Xiang, X. Guo, T. Zhou, Y. Wu, W. Xu, P. Yan, C. Wang, J.-G. Zhang, Y. Yu, ACS Appl. Mater. Interfaces 8 (2016) 16718–16726.
[6] M.M. Rahman, J.-Z. Wang, M.F. Hassan, D. Wexler, H.K. Liu, Adv. Energy Mater. 1 (2011) 212–220.
[7] M. Wagemaker, D.R. Simon, E.M. Kelder, J. Schoonman, C. Ringpfeil, U. Haake, D. Lützenkirchen-Hecht, R. Frahm, F.M. Mulder, Adv. Mater. 18 (2006) 3169–3173.
[8] X.-L. Wu, L.-Y. Jiang, F.-F. Cao, Y.-G. Guo, L.-J. Wan, Adv. Mater. 21 (2009) 2710–2714.
[9] C. Sun, S. Rajasekhara, J.B. Goodenough, F. Zhou, J. Am. Chem. Soc. 133 (2011) 2132–2135.
[10] L. Zhao, Y.-S. Hu, H. Li, Z. Wang, L. Chen, Adv. Mater. 23 (2011) 1385–1388.
[11] X. Feng, N. Ding, Y. Dong, C. Chen, Z. Liu, J. Mater. Chem. A 1 (2013) 15310–15315.
[12] J. Lu, G. Oyama, S. Nishimura, A. Yamada, Chem. Mater. 28 (2016) 1101–1106.
[13] F.C. Strobridge, H. Liu, M. Leskes, O.J. Borkiewicz, K.M. Wiaderek, P.J. Chupas, K.W. Chapman, C.P. Grey, Chem. Mater. 28 (2016) 3676–3690.
[14] W.J.H. Borghols, M. Wagemaker, U. Lafont, E.M. Kelder, F.M. Mulder, J. Am. Chem. Soc. 131 (2009) 17786–17792.
[15] D.P. Singh, F.M. Mulder, M. Wagemaker, Electrochem. Commun. 35 (2013) 124–127.
[16] C. Kim, N.S. Norberg, C.T. Alexander, R. Kostecki, J. Cabana, Adv. Funct. Mater 23 (2013) 1214–1222.
[17] H. Hain, M. Scheuermann, R. Heinzmann, L. Wünsche, H. Hahn, S. Indris, Solid State Nucl. Magn. Reson 42 (2012) 9–16.
[18] C. Wang, S. Wang, Y.-B. He, L. Tang, C. Han, C. Yang, M. Wagemaker, B. Li, Q.-H. Yang, J.-K. Kim, F. Kang, Chem. Mater. 27 (2015) 5647–5656.
[19] W. Schmidt, M. Wilkening, J. Phys. Chem. C 120 (2016) 11372–11381.
[20] W. Schmidt, M. Wilkening, Solid State Ion. 287 (2016) 77–82.
[21] B. Ziebarth, M. Klinsmann, T. Eckl, C. Elsässer, Phys. Rev. B 89 (2014).
[22] D. Massiot, F. Fayon, M. Capron, I. King, S. Le Calvé, B. Alonso, J.-O. Durand, B. Bujoli, Z. Gan, G. Hoatson, Magn. Reson. Chem. 40 (2002) 70–76.
[23] G.A. Mabbott, J. Chem. Educ. 60 (1983) 697.